Inorg. Chem. **2002**, *41*, 1436–1445

Analysis of Paramagnetic NMR Spectra of Triple-Helical Lanthanide Complexes with 2,6-Dipicolinic Acid Revisited: A New Assignment of Structural Changes and Crystal-Field Effects 25 Years Later

Nadjet Ouali,[†] Bernard Bocquet,[†] Stéphane Rigault,[†] Pierre-Yves Morgantini,[‡] Jacques Weber,[‡] and Claude Piguet*[,†]

Department of Inorganic, Analytical, and Applied Chemistry and Department of Physical Chemistry, University of Geneva, 30 quai E. Ansermet, CH-1211 Geneva 4, Switzerland

Received July 27, 2001

Variable-temperature ^{1}H and ^{13}C NMR measurements of the D_3-symmetrical triple-helical complexes $[Ln(L1\text{-}2H)_3]^{3-}$ (L1 = pyridine-2,6-dicarboxylic acid; Ln = La–Lu) show evidence of dynamic intermolecular ligand-exchange processes whose activation energies depend on the size of the metal ion. At 298 K, the use of diastereotopic probes in $[Ln(L3\text{-}2H)_3]^{3-}$ (L3 = 4-ethyl-pyridine-2,6-dicarboxylic acid) shows that fast intramolecular $P \rightleftharpoons M$ interconversion between the helical enantiomers occurs on the NMR time scale. Detailed analyses of the paramagnetic NMR hyperfine shifts according to crystal-field independent techniques demonstrate the existence of two different helical structures, one for large lanthanides (Ln = La–Eu) and one for small lanthanides (Ln = Tb–Lu), in complete contrast with the isostructurality proposed 25 years ago. A careful reconsideration of the original crystal-field-dependent analysis shows that an abrupt variation of the axial crystal-field parameter $A_2^0\langle r^2\rangle$ parallels the structural change leading to some accidental compensation effects that prevent the detection of structural variations according to the classical one-nucleus method. Crystal structures in the solid state and density functional theory calculations in the gas phase provide structural models that rationalize the paramagnetic NMR data. A regular triple-helical structure is found for small lanthanides (Ln = Tb–Lu) in which the terdentate chelating ligands are rigidly tricoordinated to the metals. A flexible and distorted structure is evidenced for Ln = La–Eu in which the central pyridine rings interact poorly with the metal ion. The origin of the simultaneous variation of structural parameters and crystal-field and hyperfine constants near the middle of the lanthanide series is discussed together with the use of crystal-field-independent techniques for the interpretation of paramagnetic NMR spectra in axial lanthanide complexes.

Introduction

Trivalent lanthanide metal ions, Ln(III), are ideal paramagnetic structural probes in supramolecular complexes and in proteins because the partially filled 4f orbitals are essentially not involved in chemical bonding leading to magnetic dots with predetermined properties.[1] The coupling between the electronic and nuclear magnetic momenta in the molecular edifices increases nuclear relaxation processes[2] and induces considerable hyperfine NMR chemical shifts associated with contact (through-bond) and pseudocontact (through-space) mechanisms.[3] Electron-induced nuclear relaxation processes have been intensively investigated, and the theoretical modeling has been refined to such an extent that Ln−nucleus distances[4,5] and electronic relaxation times[2,5,6] are

* Corresponding author. E-mail: claude.piguet@chiam.unige.ch.
[†] Department of Inorganic, Analytical, and Applied Chemistry.
[‡] Department of Physical Chemistry.

(1) (a) Geraldes, C. F. G. C. In *NMR in Supramolecular Chemistry*; Pous, M., Ed.; Kluwer Academic: Amsterdam, 1999; pp 133−154. (b) Bertini, I.; Janik, M. B. L.; Lee, Y.-M.; Luchinat, C.; Rosato, A. *J. Am. Chem. Soc.* **2001**, *123*, 4181.
(2) (a) Bertini, I.; Luchinat, C. *Coord. Chem. Rev.* **1996**, *150*, 1. (b) Sharp, R.; Lohr, L.; Miller, J. *Prog. Nucl. Magn. Reson. Spectrosc.* **2001**, *38*, 115. (c) Clementi, V.; Luchinat, C. *Acc. Chem. Res.* **1998**, *31*, 351.
(3) (a) Peters, J. A.; Huskens, J.; Raber, D. J. *Prog. Nucl. Magn. Reson. Spectrosc.* **1996**, *28*, 283. (b) Forsberg, J. H. In *Handbook on the Physics and Chemistry of Rare Earths*; Gschneidner, K. A., Eyring, L., Eds.; Elsevier: Amsterdam, 1996; Vol. 23, Chapter 153, p 1.
(4) (a) Burns, P. D.; La Mar, G. N. *J. Magn. Reson.* **1982**, *46*, 61. (b) Aime, S.; Barbero, L.; Botta, M.; Ermondi, G. *J. Chem. Soc., Dalton Trans.* **1992**, 225.
(5) Rigault, S.; Piguet, C.; Bernardinelli, G.; Hopfgartner, G. *J. Chem. Soc., Dalton Trans.* **2000**, 4587.

10.1021/ic010801i CCC: $22.00
Published on Web 02/19/2002

accessible from field-dependent measurements together with solvent relaxation enhancement induced by Gd(III) complexes.[7] On the other hand, theoretical modeling of the paramagnetic lanthanide-induced shift (Δ_{ij}) has been proposed by Golding and Halton[8] for the contact contribution (δ_{ij}^{c}) associated with through-bond spin delocalization (Fermi mechanism) and by Bleaney for the pseudocontact effect (δ_{ij}^{pc}) resulting from molecular magnetic anisotropy.[9] Taking into account that (i) the magnetic anisotropy is satisfyingly approximated by the second-order term of a T^{-n} series[10] and (ii) the crystal-field splitting does not significantly affect the projection of the electron spin magnetization of the lanthanide j onto the direction of the external field ($\langle S_z\rangle_j$),[11] eq 1 holds for predicting the paramagnetic NMR shift affecting a nucleus i in an axial complex (possessing at least a three-fold axis)[12] of a lanthanide j.[3]

$$\Delta_{ij} = \delta_{ij}^{exp} - \delta_i^{dia} = \delta_{ij}^{c} + \delta_{ij}^{pc} = \frac{F_i}{T}\langle S_z\rangle_j + \frac{G_i}{T^2}A_2^0\langle r^2\rangle C_j = F_i'\langle S_z\rangle_j + G_i'A_2^0\langle r^2\rangle C_j \quad (1)$$

C_j is a magnetic constant at a given temperature T that measures the second-order magnetic axial anisotropy of the paramagnetic lanthanide j (Bleaney's factor scaled to -100 for Dy),[9] $A_2^0\langle r^2\rangle$ is the axial crystal-field parameter, F_i is proportional to the electron−nuclear hyperfine coupling constant, and G_i is the geometric factor $(1 - 3\cos^2\theta_i)/r_i^3$ of nucleus i that contains the structural information about the complex (θ_i and r_i are the internal axial coordinates of the nucleus i with respect to the main axis (z-axis) of the magnetic susceptibility tensor, with Ln_j at the origin). In a seminal paper published in 1975, Reilley and co-workers[13] demonstrated that contact and pseudocontact contributions could be separated within an isostructural series of axial lanthanide complexes according to eqs 2 and 3 (two linear forms of eq 1) at a fixed temperature if (i) the $\langle S_z\rangle_j$ and C_j parameters tabulated for the free ions are acceptable approximations in the complexes[8,9] and (ii) F_i and $A_2^0\langle r^2\rangle$ do not vary along the lanthanide series. The original application of this method to the complexes $[Ln(Li\text{-}2H)_3]^{3-}$ (i = 1, 2; Ln = Pr, Eu, Tb−Yb; Chart 1) showed linear plots of $\Delta_{ij}/\langle S_z\rangle_j$ versus $C_j/\langle S_z\rangle_j$ (eq 2) or Δ_{ij}/C_j versus $\langle S_z\rangle_j/C_j$ (eq 3) for paramagnetic ^{1}H and ^{13}C NMR shifts along the lanthanide series, in agreement with a single rigid D_3-symmetrical

Chart 1

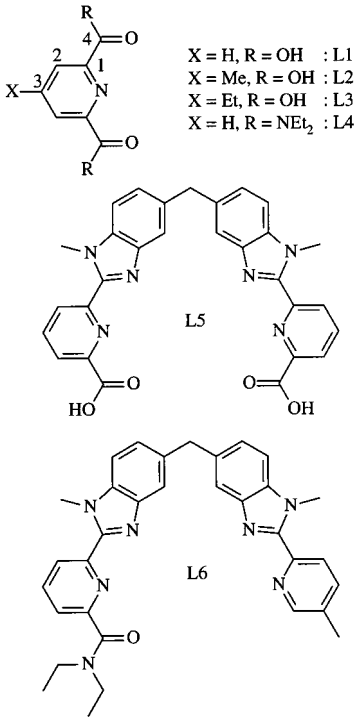

geometry for the complexes in solution (no change of G_i).[13]

$$\frac{\Delta_{ij}}{\langle S_z\rangle_j} = F_i' + G_i'A_2^0\langle r^2\rangle\frac{C_j}{\langle S_z\rangle_j} \quad (2)$$

$$\frac{\Delta_{ij}}{C_j} = F_i'\frac{\langle S_z'\rangle_j}{C_j} + G_i'A_2^0\langle r^2\rangle \quad (3)$$

Since this original contribution, breaks occurring near the middle of the series (Ln = Gd−Dy) have often been detected for closely related complexes,[3] and this recurrent behavior has been tentatively assigned to the smooth lanthanide contraction that alters G_i factors, an effect that is amplified for heavier lanthanides because of their large C_j values.[14] However, variations in F_i' and $A_2^0\langle r^2\rangle$ along the series have been recognized as valuable alternatives for rationalizing deviations from linearity according to eqs 2 and 3.[15−17] Geraldes eventually proposed eq 4, which accounts for the paramagnetic shifts of two nuclei in the same complex (Δ_{ij} and Δ_{kj}) for investigations of isostructurality along the lanthanide series.[18]

$$\frac{\Delta_{ij}}{\langle S_z\rangle_j} = (F_i' - F_k'R_{ik}) + R_{ik}\frac{\Delta_{kj}}{\langle S_z\rangle_j} \qquad R_{ik} = \frac{G_i'}{G_k'} = \frac{G_i}{G_k} \quad (4)$$

Because eq 4 does not depend on crystal-field parameters, any deviation from linearity in $\Delta_{ij}/\langle S_z\rangle_j$ versus $\Delta_{kj}/\langle S_z\rangle_j$ plots along the lanthanide series can be safely ascribed to structural

(6) (a) Alsaadi, B. M.; Rossotti, F. J. C.; Williams, R. J. P. *J. Chem. Soc., Dalton Trans.* **1980**, 2147. (b) Bertini, I.; Capozzi, F.; Luchinat, C.; Nicastro, G.; Xia, Z. *J. Phys. Chem.* **1993**, *97*, 6351.
(7) (a) Caravan, P.; Ellison, J. J.; McMurry, T. J.; Lauffer, R. B. *Chem. Rev.* **1999**, *99*, 2293. (b) Rast, S.; Borel, A.; Helm, L.; Belorizky, E.; Fries, P. H.; Merbach, A. E. *J. Am. Chem. Soc.* **2001**, *123*, 2637.
(8) Golding, R. M.; Halton, M. P. *Aust. J. Chem.* **1972**, *25*, 2577.
(9) Bleaney, B. *J. Magn. Reson.* **1972**, *8*, 91.
(10) McGarvey, B. R. *J. Magn. Reson.* **1979**, *33*, 445. Golding, R. M.; Pyykkö, P. *Mol. Phys.* **1973**, *26*, 1389. Horrocks, W. DeW., Jr. *J. Magn. Reson.* **1977**, *26*, 333.
(11) Pinkerton, A. A.; Rossier, M.; Spiliadis, S. *J. Magn. Reson.* **1985**, *64*, 420.
(12) Briggs, J. M.; Moss, G. P.; Randall, E. W.; Sales, K. D. *J. Chem. Soc., Chem. Commun.* **1972**, 1180.
(13) Reilley, C. N.; Good, B. W.; Desreux, J. F. *Anal. Chem.* **1975**, *47*, 2110.
(14) Peters, J. A. *J. Magn. Res.* **1986**, *68*, 240.
(15) Reuben, J. *J. Magn. Reson.* **1982**, *50*, 233.
(16) Ren, J.; Sherry, A. D. *J. Magn. Reson.* **1996**, *B111*, 178.
(17) Bleaney, B.; Dobson, C. M.; Levine, B. A.; Martin, R. B.; Williams, R. J. P.; Xavier, A. V. *J. Chem. Soc., Chem. Commun.* **1972**, 791.
(18) Platas, C.; Avecilla, F.; de Blas, A.; Geraldes, C. F. G. C.; Rodriguez-Blas, T.; Adams, H.; Mahia, J. *Inorg. Chem.* **1999**, *38*, 3190.

changes affecting R_{ik} (and thus G_i and G_k).[18] Applications of eq 4 to triple-stranded helicates $[Ln_2(L5\text{-}2H)_3]$ and $[LnCo(L6)_3]^{5/6+}$, in which Ln(III) are firmly held in rigid nine-coordinate tricapped trigonal prismatic sites, indeed show only straight lines along the complete lanthanide series (Ln = Ce−Yb), in agreement with isostructural behaviors, but further analyses of the data according to eqs 2 and 3 show systematic breaks between Ln = Eu and Tb that result from abrupt variations of F_i' and $A_2^0\langle r^2\rangle$ near the middle of the series.[5,19] These observations strongly suggest that specific electronic half-shell effects, sometimes referred to as the "gadolinium break" effects, are neglected in the description of paramagnetic shifts in lanthanide complexes according to eq 1.[20] Following this reasoning, the strict linear correlations reported for $[Ln(Li\text{-}2H)_3]^{3-}$ ($i = 1, 2$)[13] according to eqs 2 and 3 and assigned to a single D_3-symmetrical triple-helical structure along the complete lanthanide series are intriguing and strongly contrast with (i) the observation of two different structures for the analogous monometallic D_3-symmetrical complexes $[Ln(L4)_3]^{3+}$ (there is a break between Ln = Eu and Ln = Er)[19] and (ii) the variation of the pseudocontact contribution between large and small Ln(III) in $[Ln(L1\text{-}2H)_3]^{3-}$ reported by Williams and co-workers.[21] In this contribution, we reexamine the solution structure of $[Ln(L1-2H)_3]^{3-}$ in D_2O according to eqs 1−4 (at controlled pD and temperature), together with a three-nuclei technique,[22] eventually to assign structural changes, crystal-field effects, and variations of hyperfine constants along the lanthanide series. Particular attention has been focused on inter- and intramolecular dynamic processes occurring on the NMR time scale that affect the geometric factors.

Results and Discussion

Dynamic Behavior of $[Ln(L1\text{-}2H)_3]^{3-}$ in Solution: Intermolecular Exchange Processes. For a total ligand concentration of 0.03 M, pD = 6 (pD = pH + 0.4),[23] and a stoichiometric ratio Ln:L1 = 0.33, the calculated ligand speciation in water[24] amounts to 93% $[Ln(L1\text{-}2H)_3]^{3-}$, 5% $[Ln(L1\text{-}2H)_2]^-$, and 2% $[L1\text{-}2H]^{2-}$ (Ln = La). This ratio is 95:3:2% for Ln = Lu, thus confirming the almost quantitative formation of the triple-helical complexes $[Ln(L1\text{-}2H)_3]^{3-}$ along the complete lanthanide series. The ^{13}C NMR spectra at 298 K display four signals, corresponding to three equivalent ligand strands related by a three-fold axis, together with additional symmetry elements (three C_2 axes or a σ_h mirror plane perpendicular to the main C_3 axis) in agreement with D_3 or D_{3h} point groups on the NMR time scale. All signals have been assigned according to $\{^1H-^1H\}$ -COSY and $\{^1H-^{13}C\}$ -HETCOR correlation spectroscopy, to NOEDIFF experiments, and to paramagnetic relaxation measurements for strongly paramagnetic complexes and quaternary carbons that cannot be assigned using classical techniques.[5,21] The chemical shifts collected in Table 1 are consistent with those reported by Reilley and co-workers,[13] but a strict similitude is precluded by the different temperature used in the original study (308 K). The downfield shifts of the NMR signal of C3 ($\Delta\delta$ = 0.92, 3.48, 3.14 for Ln = La, Y, and Lu, respectively) occurring upon complexation (Table 1) are typical of *N*-coordination of the central pyridine ring, in agreement with related trends detected for H2 and H3.[25] For the large La(III), we observe broadened ^1H NMR signals at 298 K that do not change in the temperature range 283−353 K, thus pointing to an exchange process between $[La(L1\text{-}2H)_3]^{3-}$ and $[La(L1\text{-}2H)_2]^-$ occurring at a moderate rate on the NMR time scale (eq 5). For the smaller Ln = Y, Lu, the exchange process is slower, and we observe minor sets of separated signals corresponding to $[Ln(L1\text{-}2H)_2]^-$ and $[L1\text{-}2H]^{2-}$, in agreement with previous NMR studies.[21]

$$[Ln(L1\text{-}2H)_3]^{3-} \rightleftharpoons [Ln(L1\text{-}2H)_2]^- + [L1\text{-}2H]^{2-} \quad (5)$$

Increasing the total ligand concentration to 0.15 M (and the total metal concentration to 0.05 M) reduces the amount of $[Ln(L1\text{-}2H)_2]^-$ to less than 2% of the ligand species, leading to narrower signals because exchange processes between two highly unequally populated sites weakly affect NMR spectra.[26]

Addition of an excess of $[L1\text{-}2H]^{2-}$ (0.05 M) to a solution of $[La(L1\text{-}2H)_3]^{3-}$ (0.05 M) in the range 283−353 K does not provide separated signals for free and coordinated ligands, pointing to fast-exchange processes on the NMR time scale according to eq 6. For Ln = Y and Lu, the stronger Ln−ligand dative bonds reduce the exchange rate, and distinct

Table 1. Experimental ^1H and ^{13}C NMR Shifts (with Respect to DSS) for $[Ln(L1\text{-}2H)_3]^{3-}$ and $[Ln(L3\text{-}2H)_3]^{3-}$ in D_2O (298 K, pD = 6)[a]

compd	H2	H3	C1	C2	C3	C4
$[L1\text{-}2H]^{2-}$	8.00	8.00	148.57	129.71	140.44	159.06
$[La(L1\text{-}2H)_3]^{3-}$	8.16	8.24	150.48	126.83	141.36	173.08
$[Y(L1\text{-}2H)_3]^{3-}$	8.13	8.24	151.70	128.81	143.92	174.89
$[Lu(L1\text{-}2H)_3]^{3-}$	8.12	8.24	151.07	128.65	143.58	174.96
$[Ce(L1\text{-}2H)_3]^{3-}$	10.41	10.53	159.95	137.78	145.93	173.90
$[Pr(L1\text{-}2H)_3]^{3-}$	12.58	12.39	166.97	150.12	146.66	177.11
$[Nd(L1\text{-}2H)_3]^{3-}$	10.64	10.48	159.41	151.42	141.21	174.98
$[Eu(L1\text{-}2H)_3]^{3-}$	3.77	3.77	138.41	85.18	151.50	167.49
$[Tb(L1\text{-}2H)_3]^{3-}$	39.54	35.45	310.07	89.08	235.24	181.26
$[Dy(L1\text{-}2H)_3]^{3-}$	43.11	38.12	315.47	111.25	233.28	189.35
$[Ho(L1\text{-}2H)_3]^{3-}$	26.36	23.69	239.24	104.52	200.07	170.16
$[Er(L1\text{-}2H)_3]^{3-}$	−2.39	−0.75	104.92	72.40	141.69	146.88
$[Tm(L1\text{-}2H)_3]^{3-}$	−13.54	−10.35	48.88	69.31	120.78	128.72
$[Yb(L1\text{-}2H)_3]^{3-}$	0.37	1.42	111.35	109.47	134.73	155.11
$[L3\text{-}2H]^{2-}$	8.22		148.65	129.13	168.01	169.09
$[La(L3\text{-}2H)_3]^{3-}$	8.02		152.90	128.90	162.45	175.94
$[Y(L3\text{-}2H)_3]^{3-}$	7.98		151.63	128.24	162.31	175.18
$[Lu(L3\text{-}2H)_3]^{3-}$	7.98		151.18	128.25	162.13	175.41
$[Ce(L3\text{-}2H)_3]^{3-}$	10.41		160.61	137.78	164.76	174.34
$[Pr(L3\text{-}2H)_3]^{3-}$	13.04		165.53	150.41	167.50	177.31
$[Nd(L3\text{-}2H)_3]^{3-}$	10.56		159.95	151.81	170.49	175.63

[a] Sm(III) is not considered because of its weak paramagnetism.[5]

(19) Rigault, S.; Piguet, C.; Bünzli, J.-C. G. *J. Chem. Soc., Dalton Trans.* **2000**, 2045.
(20) Rigault, S.; Piguet, C. *J. Am. Chem. Soc.* **2000**, *122*, 9304.
(21) Alsaadi, B. M.; Rossotti, F. J. C.; Williams, R. J. P. *J. Chem. Soc., Dalton Trans.* **1980**, 597.
(22) Geraldes, C. F. C. G.; Zhang, S.; Platas, C.; Rodriguez-Blas, T.; de Blas, A.; Sherry, A. D. *J. Alloys Compd.* **2001**, *323*−*324*, 824.
(23) Glasoe, P. K.; Long, F. A. *J. Phys. Chem.* **1960**, *64*, 188.
(24) Grenthe, I. *J. Am. Chem. Soc.* **1961**, *83*, 360.
(25) Lavallee, D. K.; Baughman, M. D.; Phillips, M. P. *J. Am. Chem. Soc.* **1977**, *99*, 718. Annuziata, R.; Benaglia, M.; Famulari, A.; Raimondi, L. *Magn. Reson. Chem.* **2001**, *39*, 341.
(26) Pons, M.; Millet, O. *Prog. Nucl. Magn. Reson. Spectrosc.* **2001**, *38*, 267.

NMR signals are observed for free and bound ligands, as previously noticed by Williams and co-workers[21] and in complete agreement with closely related dynamic behavior reported for the analogous complexes $[Ln(L4)_3]^{3+}$ in acetonitrile.[27]

$$[Ln(L1\text{-}2H)_3]^{3-} + [L1^*\text{-}2H]^{2-} \rightleftharpoons [Ln(L1\text{-}2H)_2(L1^*\text{-}2H)]^{3-} + [L1\text{-}2H]^{2-} \quad (6)$$

Coalescence between the signals of H2 in free and coordinated ligands occurs at $T_c = 318$ K for $[Y(L1\text{-}2H)_3]^{3-}$ and $T_c = 348$ K for $[Lu(L1\text{-}2H)_3]^{3-}$, leading to free activation energies of $\Delta G^{\ddagger}(Y) = 68(1)$ kJ/mol and $\Delta G^{\ddagger}(Lu) = 74(1)$ kJ/mol, calculated with eqs 7−9 at these temperatures (k is the rate constant at T_c, $\delta\nu$ is the chemical shift difference in the absence of exchange ($\delta\nu(Y) = 37$ Hz, $\delta\nu(Lu) = 39$ Hz), k_B and h are respectively the Boltzmann and the Plank constants, Δp is the difference in the population between the two exchangeable sites ($\Delta p = 0.5$ under our stoichiometric conditions), and X is the solution of the polynomial expression given in eq 9 ($X = 2.30$ for $\Delta p = 0.5$)).[26]

$$\Delta G^{\ddagger} = RT \ln\left(\frac{k_B T}{kh}\right) \quad (7)$$

$$k = \frac{\pi\,\delta\nu}{X} \quad (8)$$

$$X^6 - 6X^4 + [12 - 27(\Delta p)^2]X^2 - 8 = 0 \quad (9)$$

As no coalescence is observed for $[La(L1\text{-}2H)_3]^{3-}$ at the lowest accessible temperature (278 K), we can estimate with eqs 7−9 and $\delta\nu(Y) = 37$ Hz that the maximum value for $\Delta G^{\ddagger}(La)$ is ≤59 kJ/mol. We thus conclude that the experimental chemical shifts δ_{ij}^{exp} measured for the complexes of the small lanthanides $[Ln(L1\text{-}2H)_3]^{3-}$ (Ln = Tb−Lu, 298 K) reflect those of the bound ligand without the complications that are due to exchange processes. For the large lanthanides (Ln = La−Eu), strict stoichiometric conditions (Ln:L1 = 0.33) combined with high concentrations are required to remove any contributions from unbound ligands in fast chemical exchange (eqs 5 and 6, Table 1). Finally, ^{1}H and ^{13}C NMR spectra recorded for $4 \le pD \le 8$ display no change at 298 K, but line broadening is detected for extreme pD domains ($pD < 4$ and $pD > 7$) in which partial decomplexation assisted by protonation or by hydroxide displacement is expected (eq 5).

Dynamic Behavior of $[Ln(L1\text{-}2H)_3]^{3-}$ in Solution: Intramolecular Exchange Processes. Variable-temperature NMR spectra of the analogous complexes $[Ln(L4)_3]^{3+}$ in acetonitrile have shown that the methylene protons of the amide sidearms are enantiotopic at 298 K for Ln = La−Eu and diastereotopic for Ln = Er−Lu, thus pointing to a dynamic process involving $P \rightleftharpoons M$ helical interconversion on the NMR time scale and whose activation energies decrease with the increasing ionic size of Ln(III) ($\Delta G^{\ddagger}(Sm) = 55$ kJ/mol ($T_c = 263$ K), $\Delta G^{\ddagger}(Y) = 73$ kJ/mol ($T_c = 318$ K), and $\Delta G^{\ddagger}(Lu) = 78$ kJ/mol ($T_c = 333$ K)).[27] According to enantioselective quenching investigations, related $P \rightleftharpoons M$ racemization processes occur for $[Ln(L1\text{-}2H)_3]^{3-}$ in water and prevent chiral resolution in the ground state ($k \approx 10$ s^{-1} has been estimated for $[Eu(L1\text{-}2H)_3]^{3-}$ in the excited state at room temperature).[28] Because no diastereotopic probe is available for $[Ln(Li\text{-}2H)_3]^{3-}$ ($i = 1, 2$), this helical interconversion cannot be detected by dynamic NMR in solution.[29] The introduction of a methylene probe at the 4-position of the pyridine ring in L3 (Scheme 1)[30] overcomes this limitation, and the triple-helical complexes $[Ln(L3\text{-}2H)_3]^{3-}$ (Ln = La−Eu, Tm, Yb, Lu, Y) display NMR spectra identical (within experimental error for common nuclei) to those obtained for $[Ln(L1\text{-}2H)_3]^{3-}$, thus pointing to comparable structures in solution (Table 1).

Scheme 1[a].

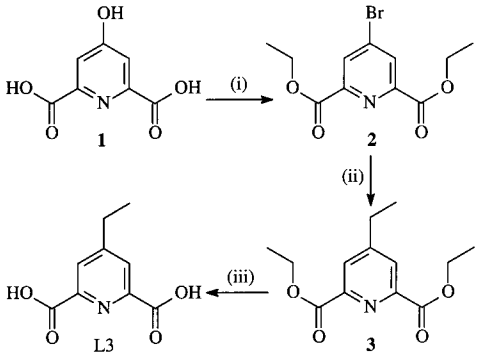

[a] Reagents: (i) (1) PBr_5 and (2) C_2H_5OH, (ii) $(C_2H_5)_2Zn$, $Pd(P(C_6H_6)_3)_2Cl_2$, THF, (iii) KOH, C_2H_5OH, H_2O

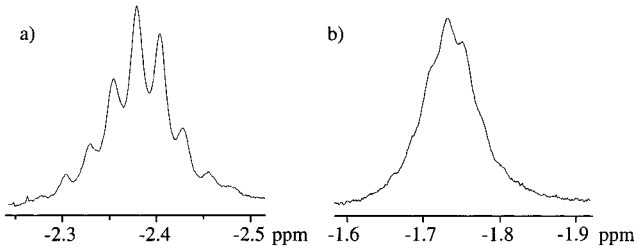

Figure 1. Part of the ^{1}H NMR spectra of $[Yb(L3\text{-}2H)_3]^{3-}$ in D_2O showing the signals of the methylene protons at (a) 283 K and (b) 303 K.

For the diamagnetic complexes $[Ln(L3\text{-}2H)_3]^{3-}$ (Ln = La, Lu, Y), the two methylene protons of the ethyl residue provide a well-resolved quartet (283−358 K) in agreement with accidental isochronicity or fast $P \rightleftharpoons M$ helical interconversion on the NMR time scale. For paramagnetic complexes $[Ln(L3\text{-}2H)_3]^{3-}$ (Ln = Eu, Tm, Yb), we observe two interpenetrated pseudosextets at 283 K corresponding to the AB part of ABX_3 spin systems, thus pointing to two diastereotopic methylene protons that coalesce into a quartet (A_2X_3 spin systems) at higher temperature (Figure 1). These observations demonstrate that a dynamic helical interconversion (eq 10; Chart 2) occurs for $[Ln(L3\text{-}2H)_3]^{3-}$ in the

(27) Renaud, F.; Piguet, C.; Bernardinelli, G.; Bünzli, J.-C. G.; Hopfgartner, G. *Chem.—Eur. J.* **1997**, *3*, 1646.

(28) Meskers, S. C. J.; Dekkers, H. P. J. M. *J. Phys. Chem. A* **2001**, *105*, 4589 and references therein. Huskowska, E.; Riehl, J. P. *Inorg. Chem.* **1995**, *34*, 5615 and references therein.

(29) Rüttimann, S.; Piguet, C.; Bernardinelli, G.; Bocquet, B.; Williams, A. F. *J. Am. Chem. Soc.* **1992**, *114*, 4230.

(30) Schmidt, B.; Elhert, D. K. *Tetrahedron Lett.* **1998**, *39*, 3999.

Chart 2

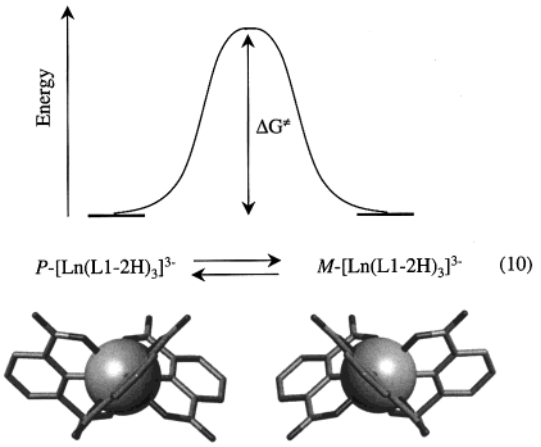

ground state on the NMR time scale along the complete lanthanide series. Paramagnetic lanthanides exhibit chemical shift differences ($\delta\nu$) between the diastereotopic methylene protons that are large enough to be displayed in the slow-exchange regime at accessible temperatures in D_2O. Considering that (i) $\delta\nu$ measured at 283 K is a rough approximation of $\delta\nu$ in absence of exchange and (ii) the paramagnetic dependence of $\delta\nu$ on temperature can be limited to the paramagnetic pseudocontact contributions, according to Bleaney's theory ($\delta\nu_{T_2} = \delta\nu_{T_1}(T_1/T_2)^2$),[9,10,31] applications of eqs 7−9 for an equally populated two-site system ($\Delta p = 0$, and $X = \sqrt{2}$)[26] give $\Delta G^{\ddagger}$(Eu) = 63(1) kJ/mol (T_c = 290 K), $\Delta G^{\ddagger}$(Tm) = 64(1) kJ/mol (T_c = 290 K), and $\Delta G^{\ddagger}$(Yb) = 60(1) kJ/mol (T_c = 303 K). The associated rate constants at 298 K can be estimated with eq 7, leading to k = 50(12), 37(11), and 200(80) s^{-1} for Ln = Eu, Tm, and Yb, respectively, which are comparable to the rate constants estimated from enantioselective quenching measurements in the excited state.[28] Compared to $[Ln(L4)_3]^{3+}$ in acetonitrile,[27] the intramolecular racemization process in $[Ln(Li\text{-}2H)_3]^{3-}$ (i = 1−3) is slightly faster, and there is no clear evidence for the dependence of $\Delta G^{\ddagger}$ on the ionic size of the metal ions (Ln = Eu−Yb). Contrary to the original reports of Donato and Martin[32] and Reilley and co-workers[13] suggesting that $[Ln(L1\text{-}2H)_3]^{3-}$ is rigid in water at 308 K, our results demonstrate that these complexes racemize ($P \rightleftharpoons M$ helical interconversion) within 10−100 ms in water (298 K, pD = 6.0), a time scale accessible to NMR measurements. For longer time scales, an average nonchiral D_{3h} symmetry is observed (for instance in chromatography) while rigid chiral D_3-symmetrical triple helices are detected for time scales in the millisecond domain or shorter (for instance, during luminescence decay). We conclude from the variable-temperature NMR studies that (i) the chemical shifts collected in Table 1 are not affected by intermolecular dynamic processes under stoichiometric conditions and (ii) the chemical shifts reflect the limiting D_3-symmetrical arrangements P-$[Ln(L1\text{-}2H)_3]^{3-}$ or M-$[Ln(L1\text{-}2H)_3]^{3-}$ that are shown in Chart 2 and correspond to the minimum of the potential energy of the racemization process.

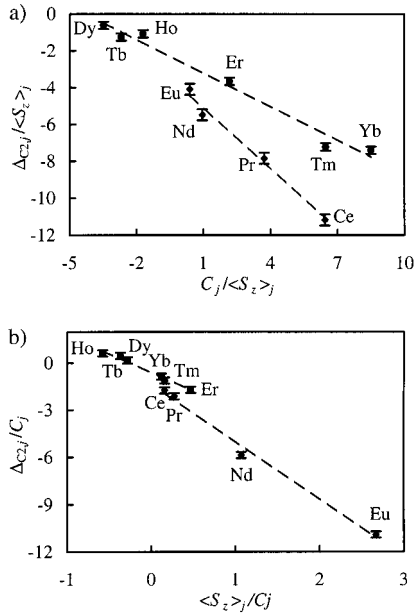

Figure 2. Plots of $\Delta_{ij}/\langle S_z\rangle_j$ vs $C_j/\langle S_z\rangle_j$ (eq 2) and Δ_{ij}/C_j vs $\langle S_z\rangle_j/C_j$ (eq 3) for C2 in $[Ln(L1\text{-}2H)_3]^{3-}$ (D_2O, 298 K, pD = 6).

Isostructurality and Crystal-Field Effects for $[Ln(L1\text{-}2H)_3]^{3-}$ in Solution. The paramagnetic contributions $\Delta_{ij} = \delta_{ij}^{exp} - \delta_i^{dia}$ that are collected in Table S1 (Supporting Information) are obtained by using $[La(L1\text{-}2H)_3]^{3-}$ as a diamagnetic reference for Ln = Ce−Nd, $[Y(L1\text{-}2H)_3]^{3-}$ for Ln = Eu−Dy, and $[Lu(L1\text{-}2H)_3]^{3-}$ for Ln = Ho−Yb.[1,33] Contrary to the original report,[13] plots of $\Delta_{ij}/\langle S_z\rangle_j$ versus $C_j/\langle S_z\rangle_j$ (eq 2) or Δ_{ij}/C_j versus $\langle S_z\rangle_j/C_j$ (eq 3) for paramagnetic ^1H and ^{13}C NMR shifts show significant deviations from linearity near the middle of the series, and two straight lines involving large (Ln = Ce−Eu) and small (Ln = Tb−Yb) lanthanides are required to fit the data (Figure 2). The resulting hyperfine terms F_i' and the products $G_i' A_2^0\langle r^2\rangle$ are collected in Table 2, together with the agreement factors $0.05 \le AF_i \le 0.22$ (eq 11)[13,27] that point to satisfying linear correlations.

$$AF_i = \sqrt{\frac{\sum_j (\Delta_{ij}^{exp} - \Delta_{ij}^{calc})^2}{\sum_j (\Delta_{ij}^{exp})^2}} \qquad (11)$$

The abrupt variations of F_i' occurring between Ln = Eu and Tb imply changes in the Fermi constants, as previously observed for closely related C_3 axial complexes $[Ln(L4)_3]^{3+}$, $[Ln_2(L5\text{-}2H)_3]$, $[LnCo(L6)_3]^{6+}$,[19] and [Ln(cryptate)],[18] but the concomitant abrupt changes of $G_i' A_2^0\langle r^2\rangle$ cannot be safely assigned to structural changes affecting G_i because of the unpredictable variations of the crystal-field parameters.[15,16,18,19] Plots of $\Delta_{ij}/\langle S_z\rangle_j$ versus $\Delta_{kj}/\langle S_z\rangle_j$ ($i \neq k$) according to the crystal-field-independent eq 4 systematically show two straight lines for Ln = Ce−Eu and Ln = Tb−Yb (Figure 3) with different slopes ($R_{ik} = G_i/G_k$, Table 3) and intercepts

(31) Desreux, J. F.; Reilley, C. N. *J. Am. Chem. Soc.* **1976**, *98*, 2105.
(32) Donato, H.; Martin, R. B. *J. Am. Chem. Soc.* **1972**, *94*, 4129.
(33) Kemple, M. D.; Ray, B. D.; Lipkowitz, K. B.; Prendergast, F. G.; Rao, B. D. N. *J. Am. Chem. Soc.* **1988**, *110*, 8275.

Table 2. Hyperfine Coupling Constants F'_i and Pseudocontact Factors $G'_i \cdot A_2^0\langle r^2\rangle$ for Protons and Carbons in $[Ln(L1\text{-}2H)_3]^{3-}$ According to Equation 1 (D_2O, 298 K, pD = 6)

compd		H2	H3	C1	C2	C3	C4
Ln = Ce−Eu	F'_i	−0.28(1)	−0.30(3)	−0.75(4)	−3.7(2)	0.98(9)	−0.6(1)
	$G'_i \cdot A_2^0\langle r^2\rangle$	−0.32(1)	−0.30(2)	−1.32(3)	−1.2(2)	−0.80(8)	−0.1(1)
Ln = Tb−Yb	F'_i	0.03(7)	0.02(6)	0.3(4)	−2.6(2)	1.2(1)	−1.2(2)
	$G'_i \cdot A_2^0\langle r^2\rangle$	−0.36(2)	−0.31(2)	−1.7(1)	−0.58(7)	−0.59(3)	−0.53(6)
	AF_i[a]	0.09	0.09	0.10	0.14	0.05	0.22
	$\frac{G_i^{Ln=Ce-Eu}}{G_i^{Ln=Tb-Yb}}$	0.51	0.60	0.45	1.08	0.89	
	$\frac{A_2^0\langle r^2\rangle^{Ln=Ce-Eu}}{A_2^0\langle r^2\rangle^{Ln=Tb-Yb}}$	1.74	1.60	1.52	1.86	1.52	

[a] Agreement factors calculated according to eq 11.

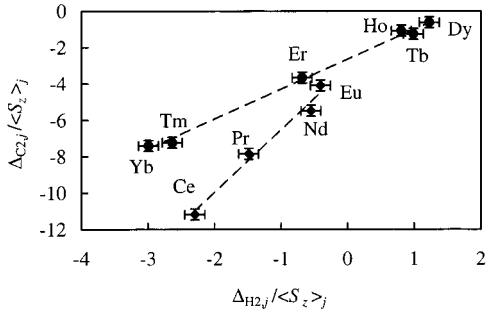

Figure 3. Plot of $\Delta_{ij}/\langle S_z\rangle_j$ vs $\Delta_{kj}/\langle S_z\rangle_j$ according to eq 4 for the H2−C2 pair in $[Ln(L1\text{-}2H)_3]^{3-}$ (D_2O, 298 K, pD = 6).

Table 3. Minimal Set of the Geometric Ratio $R_{ik} = G_i/G_k$ Obtained from Plots of $\Delta_{ij}/\langle S_z\rangle_j$ vs $\Delta_{kj}/\langle S_z\rangle_j$ According to Equation 4 for $[Ln(L1\text{-}2H)_3]^{3-}$ (D_2O, 298 K, pD = 6)[a]

	H2−H3	H2−C1	H2−C2	H2−C3	H2−C4
R_{ik} (Ce−Eu)[b]	0.98(4)	0.23(1)	0.28(3)	0.36(4)	1(1)
R_{ik} (Tb−Yb)[c]	1.15(1)	0.20(1)	0.60(2)	0.64(2)	1(5)
R_{ik} ($[La(L1\text{-}2H)_3]^{3-}$)[d]	1.13	0.22	0.53	0.65	1.22
R_{ik} ($[Lu(L1\text{-}2H)_3]^{3-}$)[d]	1.11	0.21	0.51	0.63	2.66
R_{ik} ($[La(L1\text{-}2H)_3]^{3-}$)[e]	1.18	0.23	0.55	0.68	0.84
R_{ik} ($[Lu(L1\text{-}2H)_3]^{3-}$)[e]	1.15	0.21	0.52	0.65	1.24

[a] A complete set of R_{ik} data generated according to $R_{ik} = R_{il}\,R_{lk}$ is given in the Supporting Information together with the experimental and calculated intercepts $F'_i - F'_k\,R_{ik}$ (Table S2). Errors obtained according to multilinear least-squares fits are given in parentheses. [b] Values for the first isostructural series (Sm has been removed because of its slight paramagnetism). [c] Values for the second isostructural series. [d] Calculated for the crystal structures of [Cr(sarcophagine)][Ln(L1-2H)$_3$][35] after averaging to D_3 symmetry.[34] [e] Calculated for the DFT-optimized D_3-symmetrical geometries of $[Ln(L1\text{-}2H)_3]^{3-}$ in the gas phase.

($F'_i - F'_k\,R_{ik}$, Table S2, Supporting Information), thus demonstrating that a structural change affecting G_i indeed occurs for $[Ln(L1\text{-}2H)_3]^{3-}$ between Ln = Eu and Tb. These changes were previously suggested by Williams and coworkers; they reported an abrupt variation of the $\Delta_{H2,j}/\Delta_{H3,j}$ ratio near the middle of the series.[21]

Calculations of the structural factors R_{ik} for H2, H3, and C1−C4 in the D_3-averaged crystal structures[34] of [Cr(sarcophagine)][La(L1-2H)$_3$] and [Cr(sarcophagine)][Lu(L1-2H)$_3$] (Table 3)[35] suggest that the solid-state structures do not significantly vary along the lanthanide series, except for (i) the expected 15% expansion of the Ln−O and Ln−N bonds when going from Ln = Lu to Ln = La and (ii) the associated unwrapping of the ligand strands as measured by the minor distortion (approximately 10°, vide infra) of the trigonal prism defined by the two distal oxygen tripods toward the octahedron for Ln = La. These two conditions weakly affect the R_{ik} parameters, except for C4 whose angular coordinate in the crystal structures ($\theta_{C4} = 55.9-57.6°$) is close to the magic angle (54.7°), which precludes reliable predictions of R_{ik} for pairs involving this nucleus ($G_{C^4} \approx 0$ and C4 is not considered in further structural analyses).[3,14] Calculations of the agreement factors AF_{Ln} (eq 12) that quantitatively compare the structural R_{ik} terms found for $[Ln(L1\text{-}2H)_3]^{3-}$ in solution and those calculated in the solid state for $[La(L1\text{-}2H)_3]^{3-}$ and $[Lu(L1\text{-}2H)_3]^{3-}$ amount to $AF_{La} = 0.13$ and $AF_{Lu} = 0.12$ for Ln = Tb−Yb; $AF_{La} = 0.68$ and $AF_{Lu} = 0.72$ for Ln = Ce−Eu. These results demonstrate that both crystal structures are satisfying structural models of the solution structure of the second series involving small Ln(III) atoms (Ln = Tb−Yb) but that distortions affect the solution structure of large Ln(III) atoms (Ln = Ce−Eu).

$$AF_{Ln} = \sqrt{\frac{\sum_{i\neq k}(R_{ik}^{solution} - R_{ik}^{crystal})^2}{\sum_{i\neq k}(R_{ik}^{solution})^2}} \qquad (12)$$

The extraction of geometric factors G_i for each isostructural series (eqs 2 and 3) in solution is precluded by the unknown variation of the crystal-field parameter $A_2^0\langle r^2\rangle$, and we have resorted to the a priori estimation of one G_i factor to calculate all remaining G_k geometric factors from the R_{ik} values (Table 3; eq 4). As the central pyridine ring of the ligand is coordinated to the metal in $[La(L1\text{-}2H)_3]^{3-}$ and $[Lu(L1\text{-}2H)_3]^{3-}$ in solution (downfield complexation shifts are observed for C3, Table 1),[25] we do not expect drastic variations in the Ln−C3 distance (r_{C3}) to occur, except for the lanthanide contraction, and we can estimate that $G_{C3} = (1 - 3\cos^2\theta_{C3})/(r_{C3})^3 = 0.00637$ and 0.00716 Å^{-3} for Ln = La and Lu, respectively, from the Ln−C3 distances observed in the crystal structures[35] and $\theta_{C3} = 90°$. Two sets of geometrical factors $G_i^{Ln=Ce-Eu}$ and $G_i^{Ln=Tb-Yb}$ are obtained for $[Ln(L1\text{-}2H)_3]^{3-}$ in solution (Table S3, Supporting Information), whose ratio $G_i^{Ln=Ce-Eu}/G_i^{Ln=Tb-Yb}$ gives access to the ratio of the crystal-field parameters

(34) The G_i terms of each nuclei are first calculated, and the averaging according to D_3 symmetry is then performed.

(35) Harrowfield, J. M.; Kim, Y.; Skelton, B. W.; White, A. H. *Aust. J. Chem.* **1995**, *48*, 807.

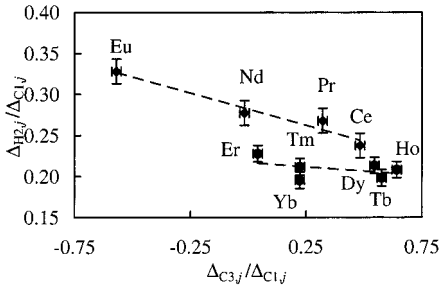

Figure 4. Plots of Δ_{ij}/Δ_{kj} vs Δ_{lj}/Δ_{kj} according to eq 13 for the H2−C1−C3 triad in $[Ln(L1\text{-}2H)_3]^{3-}$ (D_2O, 298 K, pD = 6).

$A_2^0\langle r^2\rangle^{Ln=Ce-Eu}/A_2^0\langle r^2\rangle^{Ln=Tb-Yb} = 1.6(1)$ from the $G_i'A_2^0\langle r^2\rangle$ terms of each isostructural series (Table 2). A straightforward interpretation invokes a weaker interaction between the donor atom of the ligands and Ln(III) for the small lanthanides because of the reduced spatial diffuseness of the 4f electronic orbitals.[36] However, the observation of comparable ratios of crystal-field parameters in $[Ln_2(L5-2H)_3]$ and $[LnCo(L6)_3]^{6+}$ (acetonitrile, 298 K), for which no structural changes occur, prevents definitive interpretations.[19] A similar treatment of the data reported for the closely related complexes $[Ln(L4)_3]^{3+}$ [19,27] in which a structural change occurs in acetonitrile between Ln = Eu and Er provides $A_2^0\langle r^2\rangle^{Ln=Ce-Eu}/A_2^0\langle r^2\rangle^{Ln=Er-Yb} = 3(1)$.

Geraldes and co-workers suggest removing the last free-ion parameter $\langle S_z\rangle_j$ with a three-nuclei method (eqs 13−14, nuclei *i*, *k*, *l*) for which plots of Δ_{ij}/Δ_{kj} versus Δ_{lj}/Δ_{kj} are expected to be linear within an isostructural series displaying no variation of the hyperfine constants.[22]

$$\frac{\Delta_{ij}}{\Delta_{kj}} = \alpha\frac{\Delta_{lj}}{\Delta_{kj}} + \beta \tag{13}$$

$$\alpha = \frac{\frac{F_{ij}'}{F_{kj}'} - R_{ik}}{\frac{F_{lj}'}{F_{kj}'} - R_{lk}} \quad \text{and} \quad \beta = \frac{\frac{F_{lj}'}{F_{kj}'}R_{ik} - \frac{F_{ij}'}{F_{kj}'}R_{lk}}{\frac{F_{lj}'}{F_{kj}'} - R_{lk}} \tag{14}$$

Application of this technique to triads of paramagnetic NMR shifts in $[Ln(L1\text{-}2H)_3]^{3-}$ systematically gives two straight lines for Ln = Ce−Eu and Ln = Tb−Yb, in agreement with variations of F_i' and G_i' near the middle of the lanthanide series (Figure 4). The complicated nonlinear relationships defining the slope and the intercept in eq 14 prevent direct access to the origin of the break, but simulations of the α and β parameters with R_{ik} and F_i' obtained with eqs 2−4 are in good agreement with those obtained from the experimental plots of Δ_{ij}/Δ_{kj} versus Δ_{lj}/Δ_{kj} (Table S4, Supporting Information). These results firmly establish that (i) the paramagnetic NMR shift is satisfyingly modeled by eq 1 for each isostructural series, (ii) the free-ion $\langle S_z\rangle_j$ value is an acceptable approximation for the axial complexes $[Ln(L1\text{-}2H)_3]^{3-}$ in solution, (iii) isostructurality and solution structure can be reliably investigated by eq 4, and (iv) the break occurring near the middle of the lanthanide series indeed reflects a structural change.

Molecular Structures of $[Ln(L1\text{-}2H)_3]^{3-}$ (Ln = La−Lu) in Solution by Paramagnetic NMR. The satisfying agreement observed between the R_{ik} terms of $[Ln(L1\text{-}2H)_3]^{3-}$ in solution with Ln = Tb−Yb and those calculated from the crystal structures of $[Ln(L1\text{-}2H)_3][Cr(sarcophagine]$ (Ln = La, Lu)[35] implies that the regular pseuso-D_3 symmetrical triple-helical arrangement obtained in the solid state also holds for small lanthanides in solution. A detailed geometrical analysis of the nine-coordinate, pseudotricapped, trigonal-prismatic lanthanide coordination sites based on the determinations of the angles ϕ, θ_i, and ω_i described previously for $[Ln(L4)_3]^{3+}$ (Ln = La, Eu, Figure 5)[27] shows only slight differences between $[La(L1\text{-}2H)_3]$ and $[Lu(L1\text{-}2H)_3]$ (Table S5, Supporting Information). Both coordination spheres are very close to perfect D_3 symmetry, exhibiting (i) a negligible bending of the two distal tripods (ϕ = 178−179°, ideal prism ϕ = 180°) and (ii) the standard flattening of the trigonal prism defined by the two distal oxygen tripods along the pseudo-C_3 axis (θ = 47−50° and 45−48° for Ln = La and Lu, respectively, and θ = 45−46° in $[Eu(L4)_3]^{3+}$).[27] The only noticeable discrepancies result from the expected contractions of the Ln−O and Ln−N bond distances when going from Ln = La (La−O = 2.50−2.56 and La−N = 2.64 Å) to Ln = Lu (Lu−O = 2.34−2.44 and Lu−N = 2.39−2.47 Å),[35] which produce an increased helical twist about Lu(III) and a smaller deformation of the trigonal prism (ω = 19−21 (Ln = La) and ω = 9−10° (Ln = Lu), ideal prism ω = 0 and ideal octahedron ω = 60°, Figure 6). Similar trends, induced by the lanthanide contraction, have been previously reported for related triple-helical complexes $[Ln(L4)_3]^{3+}$ (ω = 18−25 (Ln = La) and ω = 15−17° (Ln = Eu))[27] and $[LnCo(L6)_3]^{6+}$ (ω = 15−16 (Ln = La) and ω = 8−10° (Ln = Lu)),[5] but this minor alteration of the wrapping process has minute effects on the R_{ik} terms and cannot explain the second set of R_{ik} terms obtained for Ln = Ce−Eu (Table 3).

Theoretical modeling of $[La(L1\text{-}2H)_3]^{3-}$ and $[Lu(L1\text{-}2H)_3]^{3-}$ in the gas phase using density functional theory (DFT) provides optimized D_3-symmetrical structures for Ln = La and Lu that almost perfectly fit the crystal structures (Tables S5) and lead to very similar calculated R_{ik} terms (Table 3). Optimization processes performed with one supplementary water molecule show it to weakly interact via hydrogen bonds with the oxygen atoms of the coordinated carboxylate groups. The associated DFT-optimized geometry is slightly distorted, but we do not observe interactions between the water molecule and the metal in the first coordination sphere. These results are in line with molecular dynamics calculations performed on $[Eu(L1\text{-}2H)_3]^{3-}$;[37] the nine-coordinate complex is the only species in solution except for short period of time when one water molecule enters the first coordination sphere (average number of water molecules in the first coordination sphere = 0.17).[37] This modeling agrees with (i) detailed luminescence studies of [Eu(L1-

(36) Hopkins, T. A.; Metcalf, D. H.; Richardson, F. S. *Inorg. Chem.* **1998**, *37*, 1401.

(37) An, Y.; Berry, M. T.; van Veggel, F. C. J. M. *J. Phys. Chem. A* **2000**, *104*, 11243.

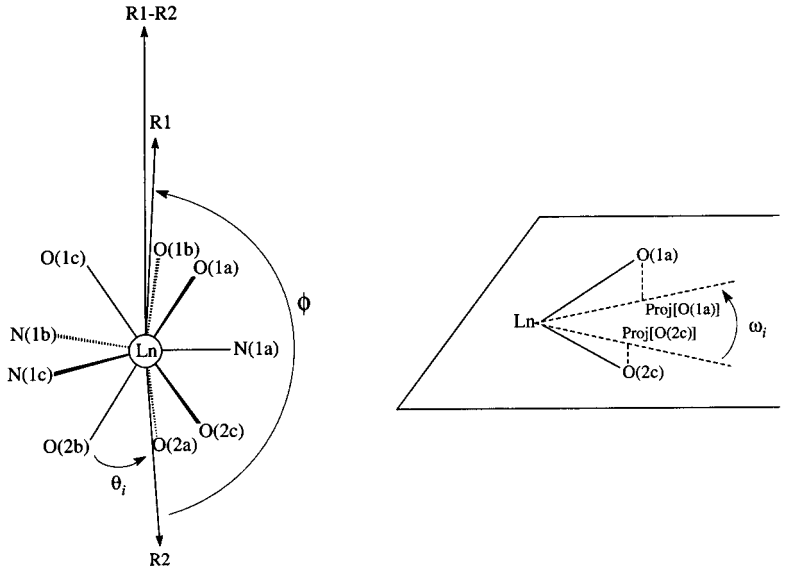

Figure 5. Definition of ϕ, θ_i, and ω_i for a pseudotricapped trigonal prismatic site (R1 = Ln−O1a + Ln−O1b + Ln−O1c and R2 = Ln−O2a + Ln−O2b + Ln−O2c). Proj[$N(i)$] is the projection of $N(i)$ along the R1−R2 direction onto a perpendicular plane passing through the metal.[27]

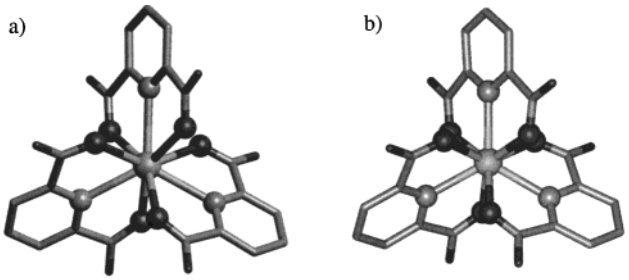

Figure 6. Views of the crystal structures of (a) $[La(L1\text{-}2H)_3]^{3-}$ and (b) $[Lu(L1\text{-}2H)_3]^{3-}$ [35] along the pseudo-C_3 axis showing the slightly different wrapping of the ligand strands.

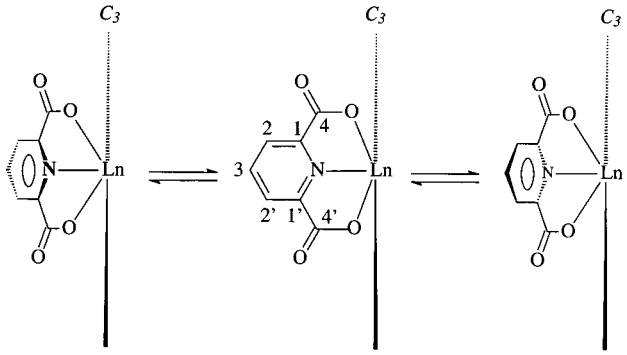

Figure 7. Oscillations of the pyridine rings in the complexes of $[Ln(L1\text{-}2H)_3]^{3-}$ with large lanthanides (Ln = Ce−Eu).

$2H)_3]^{3-}$ in which the observed long lifetime of the Eu-centered excited state in water ($\tau_{Eu}(^5D_0) = 1.67$ ms)[37] mainly reflects outer-sphere interactions with water molecules and (ii) ^{1}H NMR relaxation data that indicate that there is no water molecule in the first coordination sphere along the complete lanthanide series.[38] We conclude that the observed structural difference between large and small Ln(III) in $[Ln(L1\text{-}2H)_3]^{3-}$ does not result from the attachment of an extra water molecule to the metal for Ln = Ce−Eu, but we cannot exclude the possibility that second-sphere interactions involving solvent molecules could be responsible for distortions in the latter case. A careful examination of the crystal structures of the closely related complexes $[Ln(L4)_3]^{3+}$ (Ln = La, Eu)[27] shows that the increase of the ionic size when going from Ln = Eu to Ln = La is associated with a torsion of the central pyridine rings out of the plane of the coordinating NOO atoms of the chelating unit, which is measured by a concomitant antiphase increase of the two dihedral angles $|\alpha(O-C4-C1-N)| = 26.8-43.8°$ ($\alpha = 0$ for perfect C_2-symmetrical ligand strands, Figure 7). Such distortions remove the C_2 axes, leading to two different environments for H2 and H2′ (and C1,1′, C2,2′, and C4,4′, Figure 7) that strongly affect the associated R_{ik} terms because both r_i and θ_i vary. Calculations of the R_{ik} terms for each nucleus in the crystal structure of $[La(L4)_3]^{3+}$ provide minor difference between $R_{H2,C1}$ and $R_{H2',C1'}$ (0.10−0.25) but strongly alter $R_{H2,H3}$, $R_{H2,C2}$, and $R_{H2,C3}$ which vary between 0.5 and 1.7, 0.3 and 0.6, and 0.3 and 0.9, respectively. Because a fast "flip-flop" process of the pyridine ring is observed on the NMR time scale (average D_3 symmetry, Figure 7), only the average values of the G_i factors can be detected, leading to average R_{ik} values of 0.2, 0.4, and 0.6, respectively. These values are slightly different from those calculated for the rigid D_3-symmetrical arrangement of the pyridine observed in the crystal structure because G_i factors are nonlinear functions of θ_i and r_i. The global reductions of $R_{H2,C2}$ and $R_{H2,C3}$ are in line with the smaller R_{ik} values observed for large Ln(III) atoms in solution, which strongly suggests that a related distortion of the pyridine ring is partially responsible for the structural change occurring in solution for $[Ln(L1\text{-}2H)_3]^{3-}$ when Ln = Ce−Eu. Simulations of R_{ik} values found for structures derived from the DFT-optimized geometry found for $[La(L1\text{-}2H)_3]^{3-}$ with fixed antiphase dihedral angles $0 \le |\alpha(O-C4-C1-N)| \le 46°$ confirm this trend (Table S6, Supporting Information), but satisfying fits for $R_{H2,C2}$ and $R_{H2,C3}$ require large angular distortions ($\alpha > 46°$) that are difficult to ascribe to acceptable

(38) Alsaadi, B. M.; Rossotti, F. J. C.; Williams, R. J. P. *J. Chem. Soc., Dalton Trans.* **1980**, 813.

distortions in solution. Because the $\langle S_z\rangle_j$ values for the large Ln(III) atoms (particularly for Ln = Ce, Pr, Nd) are small compared to those of the second part of the lanthanide series,[9] we suspect that the uncertainties affecting the $\Delta_{ij}/\langle S_z\rangle_j$ terms used in eq 4 are significantly larger for Ln = Ce−Eu, thus leading to considerable errors in R_{ik}. As deviations of $\langle S_z\rangle_j$ from the free-ion value in the complexes require detailed crystal-field splittings that are not accessible for $[Ln(L1\text{-}2H)_3]^{3-}$,[39] no attempt has been made to better model the uncertainties affecting R_{ik}. However, the unambiguous observation of a break near the middle of the series according to the three methods (eqs 2, 4, and 13) confirms that the use of centroids for $\Delta_{ij}/\langle S_z\rangle_j$ in eq 4 is justified, although an exact fit with the structural model for large Ln(III) atoms is limited. A second set of G_i has been determined for the large Ln(III) atoms by using G_{C3} of the distorted structural model ($|\alpha(O-C4-C1-N)| = 32°$, Table S3, Supporting Information). The associated $G_i^{Ln=Ce-Eu}/G_i^{Ln=Tb-Yb}$ ratios only slightly deviate from those obtained when the crystal structure of $[La(L1\text{-}2H)_3]^{3-}$ is used as a reference,[35] thus leading to similar ratios of crystal-field parameters $A_2^0\langle r^2\rangle^{Ln=Ce-Eu}/A_2^0\langle r^2\rangle^{Ln=Tb-Yb} = 1.5(1)$ (Table S7, Supporting Information). We thus conclude that the increased ionic radii in Ln = Ce−Eu provide weaker Ln−ligand interactions[24] and larger flexibility of the ligand strands, leading to dynamic distortions. Of these distortions, fast oscillations of the pyridine ring on the NMR time scale qualitatively rationalize the solution structure with large Ln(III) atoms.

Conclusions

The combination of the two-nuclei (eq 4)[18] and three-nuclei (eq 13)[22] techniques developed by Geraldes gives unambiguous evidence of a structural change occurring between Ln = Eu and Tb for $[Ln(L1\text{-}2H)_3]^{3-}$ in water, in agreement with (i) the variation of pseudocontact contributions reported by Williams and co-workers[21] and (ii) the similar behavior observed for the closely related triple-helical complexes $[Ln(L4)_3]^{3+}$ in acetonitrile.[27] However, this conclusion strongly contrasts with the original conclusion presented by Reilley and co-workers, who proposed the existence of a single isostructural series according to the one-nucleus technique (eqs 1−3).[13] This apparent contradiction can be solved by the two following arguments. (1) Reilley and co-workers consider Ln = Pr and Eu only in the first lanthanide series, which provides too limited a set of data by which to assign different structures to large and small Ln(III) atoms. A brief survey of the linear plots obtained from the three techniques (Figures 2−4) clearly shows that removing the data of Ln = Nd and Ln = Ce prevents the unambiguous observation of a structural change. (2) The structural change occurring near the middle of the series (affecting the structural terms G_i) is associated with a concomitant variation of the crystal-field parameters $A_2^0\langle r^2\rangle$, which produces compensation effects in the pseudocontact terms $G_i'A_2^0\langle r^2\rangle$, thus leading to similar values along the complete lanthanide series for H2, H3, and C3 (Table 2). This effect is less pronounced for C1 and C2, which exhibit larger breaks according to eqs 2−3 (Figure 2) and cannot be treated as a single isostructural series, as demonstrated by the improvement of the agreement factor that decreases from $AF_{C2} = 0.22$ for a single isostructural series Ln = Ce−Yb to $AF_{C2} = 0.14$ for two series (Ln = Ce−Eu and Tb−Yb). Moreover, the abrupt change of the hyperfine constants F_i' also contributes to the deviation from linearity near the middle of the lanthanide series for the three techniques. Because the structural change affects the geometry and the electronic structure of the $[Ln(L1\text{-}2H)_3]^{3-}$ complexes in solution, the origin of the concomitant variations of F_i' and $A_2^0\langle r^2\rangle$ does not need further justification. It is, however, worth noting that related concomitant variations of F_i' and $A_2^0\langle r^2\rangle$ with comparable magnitudes have been observed in C_3-symmetrical triple-stranded helicates $[Ln_2(L5\text{-}2H)_3]$[19] and $[LnCo(L6)_3]^{5/6+}$ [5,20] and cryptates [Ln(crypt)][18,22] for which no structural variation is involved. We can thus not exclude the possibility that a similar gadolinium break effect[20] contributes to the variations of the hyperfine constants and the crystal-field parameters in $[Ln(L1\text{-}2H)_3]^{3-}$. Interestingly, the detailed variable-temperature NMR studies of $[Ln(L3\text{-}2H)_3]^{3-}$ show that ground-state $P \rightleftharpoons M$ helical interconversion occurs within 10−100 ms in water, a limiting lifetime for chiral resolution on the laboratory scale. Attempts to correlate the structural R_{ik} factors to solution structures demonstrate that the ligand strands are rigidly wrapped around small Ln(III) atoms (Ln = Tb−Yb) in $[Ln(L1\text{-}2H)_3]^{3-}$, thus leading to regular triple-helical complexes similar to those observed in the solid state or modeled in the gas phase. On the other hand, a larger flexibility characterizes the analogous complexes with Ln = Ce−Eu in which fast oscillation of the central pyridine ring combined with other dynamic distortions are involved. Because optimized geometries in the gas phase do not reflect these distortions, we suspect that water molecules play a crucial role in interactions with anionic complexes, in agreement with molecular dynamics calculations,[37] thus providing some driving forces for the dynamic distortions of the ligand strands.

Experimental Section

Solvents and Starting Materials. These were purchased from Aldrich, Fluka AG, and Glaser AG and used without further purification, unless otherwise stated. Dichloromethane was distilled from CaH_2, and THF, from Na. Silica gel (Brunschwig, silica 32−63, 60 Å) was used for preparative column chromatography. Diethyl-4-bromo-2,6-pyridinedicarboxylate (**2**) was prepared according to a literature procedure.[40] The triflate salts $Ln(CF_3SO_3)_3 \cdot nH_2O$ (Ln = La, Eu, Lu, Y) were prepared from the corresponding oxides (Rhodia, 99.99%) and dried according to published procedures.[41] The Ln content of the solid salts was determined by complexometric titrations with Titriplex III (Merck) in the presence of urotropine and xylene orange.

(39) Hopkins, T. A.; Bolender, J. P.; Metcalf, D. H.; Richardson, F. S. *Inorg. Chem.* **1996**, *35*, 5356.

(40) Takalo, H.; Kankare, J. *Acta Chem. Scand.* **1987**, *B41*, 219. Takalo, H.; Pasanan, P.; Kankare, J. *Acta Chem. Scand.* **1988**, *B42*, 373.

(41) Desreux, J. F. In *Lanthanide Probes in Life, Chemical, and Earth Sciences*; Bünzli, J.-C. G., Choppin, G. R., Eds.; Elsevier: Amsterdam, 1989; Chapter 2, p 43.

Syntheses and Characterizations. (a). Diethyl-4-ethyl-2,6-pyridinedicarboxylate (3). Diethyl-4-bromo-2,6-pyridinedicarboxylate (**2**) (2.17 g, 7.2 mmol) and $Pd(P(C_6H_6)_3)_2Cl_2$ (774 mg, 1.08 mmol) were dissolved in dry THF (145 cm^3) under an inert atmosphere (N_2). The yellow solution was cooled (−78 °C), diethyl zinc in toluene (7.86 cm^3, 1.1M, 8.65 mmol) was slowly added under vigorous stirring, and the mixture was maintained at these conditions for 18 h. The mixture was allowed to warm to room temperature for 19 h, and after evaporation of the solvent, the residue was partitioned between half-saturated aqueous NH_4Cl (200 cm^3) and CH_2Cl_2 (200 cm^3). The organic layer was separated, the aqueous phases were extracted with CH_2Cl_2 (3 × 200 cm^3), and the combined organic phase was dried (Na_2SO_4) and evaporated. The crude product was purified by column chromatography (silica gel, CH_2Cl_2/hexane 4:1−9:1) to give 1.013 g (4.03 mmol, yield 56%) of **3** as a pale yellow oil. NMR δ_H ($CDCl_3$): 1.29 (3H, t, ^3J = 7 Hz), 1.42 (6H, t, ^3J = 7 Hz), 2.78 (2H, q, ^3J = 7 Hz), 4.45 (4H, q, ^3J = 7 Hz), 8.39 (2H, s). IR (KBr): 1720 (C═O), 1580 cm^{-1} (C═C and C═N). EIMS *m*/*z*: 252 ($[M + H]^+$).

(b). Diethyl-4-ethyl-2,6-pyridinedicarboxylic Acid (L3). Diethyl-4-ethyl-2,6-pyridinedicarboxylate (**3**, 1.01 g, 4.02 mmol) and KOH(aq) (50 cm^3, 3 M, 0.15 mol) were dissolved in ethanol (50 cm^3). The mixture was refluxed for 2 h under an inert atmosphere. Ethanol was evaporated under vacuum, and the remaining solution was extracted with dichloromethane (2 × 150 cm^3). The aqueous phase was neutralized with half-concentrated HCl(aq) (pH 2−2.5) and concentrated under vacuum until crystallization started. The mixture was cooled to 5 °C overnight, and the white crystals were collected by filtration to give 567 mg of L3 (2.9 mmol, yield 72%); mp 182−183 °C. NMR δ_H (D_2O): 0.91 (3H, t, ^3J = 7 Hz), 2.44 (2H, q, ^3J = 7 Hz), 7.54 (2H, s); $\delta_C\{^1H\}$: 14.63, 28.78, 125.68, 153.70, 157.48, 174.23. IR (KBr): 3300 (OH), 1730 (C═O), 1600 cm^{-1} (C═C and C═N). EIMS *m*/*z*: 195 (M^+). Anal. Calcd for $C_9H_9O_4N$: C, 55.38; H, 4.62; N, 7.18. Found: C, 55.17; H, 4.86; N, 7.12.

Preparation of the Complexes $[Ln(L1\text{-}2H)_3]^{3-}$ and $[Ln(L3\text{-}2H)_3]^{3-}$ in D_2O. L*i* (*i* = 1, 3; 0.105 mmol), $[Ln(TfO)_3{\cdot}nH_2O]$ (0.035 mmol), and NaOH (0.21 mmol) were stirred in water at room temperature for 2 h to give a clear solution. The solvent was evaporated to dryness, and the solid residue was dried under vacuum (60 °C) for 12 h. D_2O (0.7 cm^3) was added, the pD was adjusted to 6 with a solution of NaOD (0.4 M, typically 0.01 mL), and the complexes $[Ln(L1\text{-}2H)_3]^{3-}$ and $([Ln(L3\text{-}2H)_3]^{3-}$ (0.05 M in D_2O) were transferred into NMR tubes.

Spectroscopic and Analytical Measurements. IR spectra were obtained from KBr pellets with a Perkin-Elmer 883 spectrometer. ^1H and ^{13}C NMR spectra were recorded at 298 K in D_2O on Broadband Varian Gemini 300 and Bruker AVANCE DRX400 spectrometers. Chemical shifts were given in ppm with respect to the internal standard DSS (2,2-dimethyl-2-silapentan-5-sulfonate), and methanol was used for temperature calibration.[42] EIMS (70 eV) spectra were recorded with VG-7000E and Finnigan-4000 instruments. Elemental analyses were performed by Dr. H. Eder at the microchemical laboratory of the University of Geneva.

Computational Details. The geometries of $[La(L1\text{-}2H)_3]^{3-}$ and $[Lu(L1\text{-}2H)_3]^{3-}$ were fully optimized at the DFT level using the nonlocal corrections of Perdew and Wang[43] for exchange and correlation functionals, as implemented in the Gaussian 98 package.[44] For all calculations, the DZVP double-ζ basis set developed by Godbout and co-workers[45] was used for the H, C, and O atoms. The lanthanide cations were described by the quasi-relativistic pseudopotential of Dolg and co-workers[46] for the 46 + 4f^n core electrons and by a (7s, 6p, 5d)/(5s, 4p, 3d) Gaussian basis set for the valence electrons. All the calculations have been performed on a Silicon graphics O2 workstation and on a cluster of PCs.

Acknowledgment. This work is dedicated to Professor J. F. Desreux. We thank Dr. D. Jeannerat for fruitful discussions. This work is supported through grants from the Swiss National Science Foundation.

Supporting Information Available: Tables of paramagnetic contributions (Table S1), geometric ratios R_{ik}, intercepts ($F_i' - F_k'R_{ik}$) (Table S2), structural G_i parameters (Table S3), and α and β parameters (Table S4) for $[Ln(L1\text{-}2H)_3]^{3-}$ in D_2O. Structural data for the lanthanide coordination spheres in $[Ln(L1\text{-}2H)_3]^{3-}$ (Ln = La, Lu) in the solid state and in the gas phase (Table S5). Table S6 reports R_{ik} calculated for structural models of large Ln(III) atoms, and Table S7 compares ratios of geometric factors and crystal-field parameters obtained from different structural models for $[Ln(L1\text{-}2H)_3]^{3-}$ (Ln = Ce−Eu). This material is available free of charge via the Internet at http://pubs.acs.org.

IC010801I

(42) Raiford, D. S.; Fisk, C. L.; Becker, E. D. *Anal. Chem.* **1979**, *51*, 2050.
(43) Perdew, J. P.; Wang, Y. In *Electronic Structure of Solids*; Ziesche, P., Eschrig, H. Eds.; Akademie Velag: Berlin, 1991; p 11.
(44) Frisch, M. J.; Trucks, G. W.; Schlegel, H. B.; Scuseria, G. E.; Robb, M. A.; Cheeseman, J. R.; Zakrzewski, V. G.; Montgomery, J. A., Jr.; Stratmann, R. E.; Burant, J. C.; Dapprich, S.; Millam, J. M.; Daniels, A. D.; Kudin, K. N.; Strain, M. C.; Farkas, O.; Tomasi, J.; Barone, V.; Cossi, M.; Cammi, R.; Mennucci, B.; Pomelli, C.; Adamo, C.; Clifford, S.; Ochterski, J.; Petersson, G. A.; Ayala, P. Y.; Cui, Q.; Morokuma, K.; Malick, D. K.; Rabuck, A. D.; Raghavachari, K.; Foresman, J. B.; Cioslowski, J.; Ortiz, J. V.; Stefanov, B. B.; Liu, G.; Liashenko, A.; Piskorz, P.; Komaromi, I.; Gomperts, R.; Martin, R. L.; Fox, D. J.; Keith, T.; Al-Laham, M. A.; Peng, C. Y.; Nanayakkara, A.; Gonzalez, C.; Challacombe, M.; Gill, P. M. W.; Johnson, B. G.; Chen, W.; Wong, M. W.; Andres, J. L.; Head-Gordon, M.; Replogle, E. S.; Pople, J. A. *Gaussian 98*, revision A.7; Gaussian, Inc.: Pittsburgh, PA, 1998.
(45) Godbout, N.; Salahub, D. R.; Andzelm, J.; Wimmer, E. *Can. J. Chem.* **1992**, *70*, 560.
(46) Dolg, M.; Stoll, H.; Savin, A.; Preuss, H. *Theor. Chim. Acta* **1989**, *75*, 173. Dolg, M.; Stoll, H.; Savin, A.; Preuss, H. *Theor. Chim. Acta* **1993**, *85*, 441.